Progress Report on Topology and Shape Optimization in Magnetostatics *

Dalibor Lukáš

Special Research Programme SFB F013
"Numerical and Symbolic Scientific Computing"
University of Linz, Austria

e-mail: dalibor.lukas@vsb.cz

Abstract

This report summarizes research results of the author achieved in the SFB subproject F1309 during the period January–September 2004. The main focus here is devoted to a development of fast multilevel methods for topology and shape optimization governed with the nonlinear magnetostatics, when using the nested approach. We also present some issues oriented to geometric or symbolic SFB subprojects. Main results are to be published in Lukáš [10] and Lukáš and Chalmovianský [11].

1 Benchmark problem

Throughout the report all the numerics is applied to the following benchmark problem. We consider a direct electric current (DC) electromagnet, see Fig. 1. The electromagnets are used for measurements of Kerr magnetooptic effects, cf. Zvedin and Kotov [17]. They require the magnetic field among the pole heads as homogeneous, i.e. as constant as possible. Let us note that the magnetooptic effects are investigated for applications in high capacity data storage media, like development of new media materials for magnetic or compact discs recording. Let us also note that the electromagnets have been developed at the Institute of Physics, Technical University of Ostrava, Czech Republic, see Postava et al. [13]. A number of instances have been delivered to laboratories in France, Canada or Japan.

Our aim is to improve the current geometries of the electromagnets in order to be better suited for measurements of the Kerr effect. The generated magnetic

*This research has been supported by the Austrian Science Fund FWF within the SFB "Numerical and Symbolic Scientific Computing" under the grant SFB F013, subproject F1309.

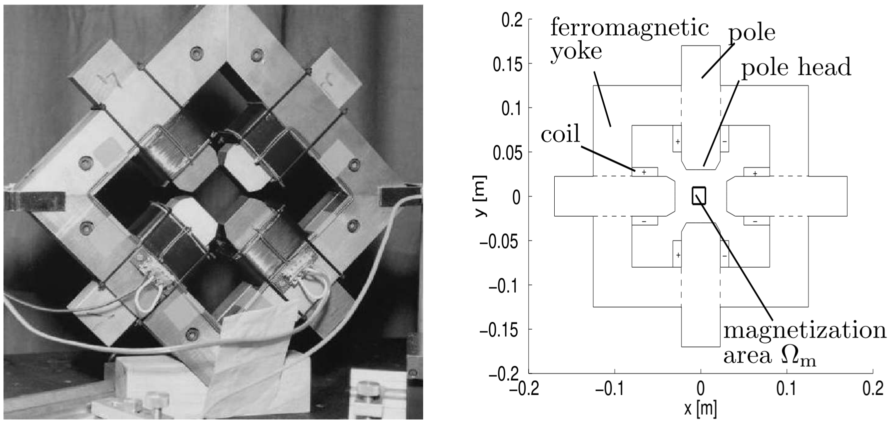

Figure 1: An electromagnet of the Maltese Cross geometry

field should be strong and homogeneous enough. Unfortunately, these assumptions are contradictory and we have to balance them. The cost functional reads as follows:

$$\mathcal{I}(\mathbf{curl}(\mathbf{u})) := \int_{\Omega_\mathrm{m}} \|\mathbf{curl}(\mathbf{u}) - B_\mathrm{m}^\mathrm{avg}\mathbf{n}_\mathrm{m}\|^2 + \xi \left(\min\{0, B_\mathrm{m}^\mathrm{avg} - B^\mathrm{min}\}\right)^2, \quad (1)$$

where $\Omega_\mathrm{m} \subset \Omega$ is the subdomain where the magnetic field should be homogeneous, $B_\mathrm{m}^\mathrm{avg}$ is the mean value over Ω_m of the magnetic flux density in the direction $\mathbf{n}_\mathrm{m} := (0, 1)$, $B^\mathrm{min} := 0.12\,[\mathrm{T}]$ is the minimal required magnitude and ξ is the related penalty which is typically $\xi := 10^6$. There are 600 turns pumped by the current of 5 [A]. The relative permeability of the used ferromagnetics is 5100. Some results were already presented in Lukáš [8] and Lukáš [9].

2 Topology optimization

We treated topology optimization governed by a nonlinear magnetostatic problem. Let us consider a fixed computational domain $\Omega \subset \mathbb{R}^d$, where $d = 2, 3$. Let $\Omega_\mathrm{d} \subset \Omega$ be the subdomain where the designed structure can arise. The set of admissible material distributions is denoted by

$$\mathcal{Q} := \{\rho \in L^2(\Omega_\mathrm{d}) \mid 0 \le \rho \le 1 \text{ a.e. in } \Omega_\mathrm{d}\}.$$

We will penalize the intermediate values as follows:

$$\widetilde{\rho}_p(\rho) := \frac{1}{2}\left(1 + \frac{1}{\arctan(p)}\arctan(p(2\rho - 1))\right), \quad p > 0,$$

which, unlike Solid Isotropic Material with Parameterization (SIMP) nor Rational Approximation of Material Properties (RAMP), cf. Bendsøe [2] or Borrvall [3], penalizes 0 and 1 equally, see also Fig. 2. Further, we consider the

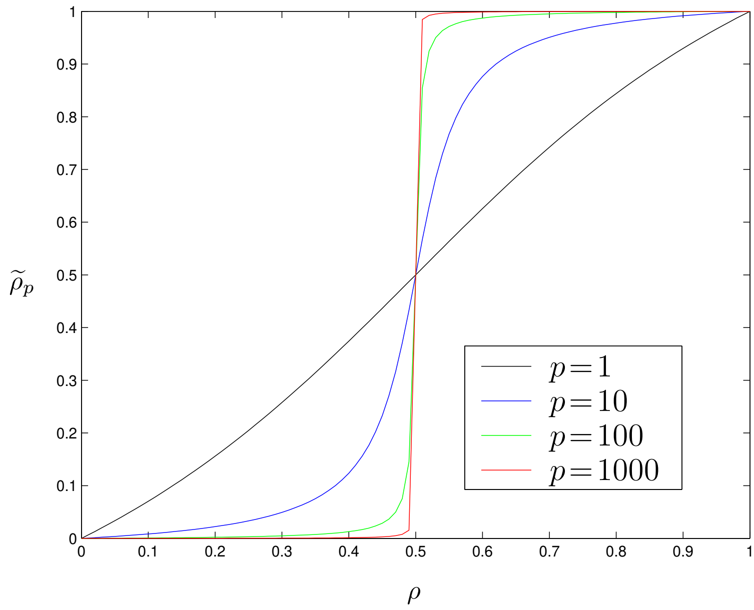

Figure 2: Penalization of intermediate values

following nonlinear magnetic reluctivity:

$$\nu(\eta, \widetilde{\rho}) := \begin{cases} \nu_0 + (\nu(\eta) - \nu_0)\widetilde{\rho}, & \text{in } \Omega_{\mathrm{d}} \\ \nu_0, & \text{otherwise,} \end{cases}$$

where $\nu(\eta) := \nu_1 + (\nu_0 - \nu_1)\frac{\eta^8}{\eta^8 + \nu_0^{-1}}$ is due to Křížek and Neittaanmäki [7], p. 134, and ν_0, ν_1 are the reluctivities of the air and ferromagnetics, respectively. Finally, we consider a cost functional $\mathcal{I} : \mathbf{L}^2(\Omega) \times \mathcal{Q} \mapsto \mathbb{R}$, possibly involving penalization of state constraints. Given a maximal volume $V_{\max}$ of the designed structure, the 3-dimensional (3d) topology optimization problem governed by the nonlinear magnetostatics then reads as follows:

$$\left\{ \begin{array}{c} \min_{\rho \in \mathcal{Q}} \mathcal{I}(\mathbf{curl}(\mathbf{u}), \widetilde{\rho}(\rho)) \\ \text{w.r.t.} \\ \int_{\Omega_{\mathrm{d}}} \widetilde{\rho}(\rho)\, d\mathbf{x} \leq V_{\max} \\ \int_{\Omega} \nu\left(\|\mathbf{curl}(\mathbf{u})\|, \widetilde{\rho}(\rho)\right) \mathbf{curl}(\mathbf{u}) \cdot \mathbf{curl}(\mathbf{v})\, d\mathbf{x} = \int_{\Omega} \mathbf{J} \cdot \mathbf{v}\, d\mathbf{x} \text{ in } \mathbf{H}_{0,\perp}(\mathbf{curl}; \Omega), \end{array} \right. \tag{2}$$

where $\mathbf{J} \in \mathbf{L}^2(\Omega)$ is a divergence-free current density and where the ansatz space $\mathbf{H}_{0,\perp}(\mathbf{curl}; \Omega)$ contains such functions $\mathbf{v} \in \mathbf{L}^2(\Omega)$ that, in a weak sense, $\mathbf{curl}(\mathbf{v}) \in \mathbf{L}^2(\Omega)$ and $\mathbf{n} \times \mathbf{v} = \mathbf{0}$ along $\partial\Omega$ and that are additionaly $\mathbf{L}^2$-orthogonal to the kernel of $\mathbf{curl}$.

The problem (2) can be reduced to 2 dimensions (2d) as follows:

$$\left\{\begin{array}{ll} & \min_{\rho\in\mathcal{Q}^{2\mathrm{d}}} \mathcal{I}\left(\left(-\frac{\partial u}{\partial x_2}, \frac{\partial u}{\partial x_1}, 0\right), \widetilde{\rho}(\rho)\right) \\ \text{w.r.t.} & \\ & \int\limits_{\Omega_{\mathrm{d}}^{2\mathrm{d}}} \widetilde{\rho}(\rho)\, d\mathbf{x} \leq A_{\max} \\ & \int\limits_{\Omega^{2\mathrm{d}}} \nu\left(\|\mathbf{grad}(u)\|, \widetilde{\rho}(\rho)\right) \mathbf{grad}(u)\cdot\mathbf{grad}(v)\, d\mathbf{x} = \int\limits_{\Omega^{2\mathrm{d}}} Jv\, d\mathbf{x} \text{ in } \mathbf{H}_0^1(\Omega^{2\mathrm{d}}), \end{array}\right. \tag{3}$$

under formally introduced assumptions that $\mathbf{u}(x_1, x_2, x_3) = (0, 0, u(x_1, x_2))$, $\mathbf{J}(x_1, x_2, x_3) = (0, 0, J(x_1, x_2))$ in a proper cut $\Omega^{2\mathrm{d}}$ of Ω, where $\Omega_{\mathrm{d}}^{2\mathrm{d}} := \Omega_{\mathrm{d}} \cap \Omega^{2\mathrm{d}}$, $\mathcal{Q}^{2\mathrm{d}}$ is the 2d conterpart of $\mathcal{Q}$ and $A^{\max}$ is a maximal admissible area of the design structure.

2.1 Numerical solution and results

The problem (2) is discretized by the finite element method using the lowest order edge Nédélec elements on tetrahedra, while we use the lowest order nodal Langrange elements on triangles in case of the 2d reduced problem. The design material distribution is elementwise constant. This leads to the following nonlinear system of equations:

$$\mathbf{A}(\mathbf{u}, \widetilde{\boldsymbol{\rho}}) \cdot \mathbf{u} = \mathbf{f},$$

where $\mathbf{u} \in \mathbb{R}^n$ and $\widetilde{\boldsymbol{\rho}} \in \mathbb{R}^m$ are the vector counterparts of the discretized solution u and the penalized design $\widetilde{\rho}$, respectively, where n, m denote the numbers of the nodes and of the elements, respectively, and where $\mathbf{A}(\mathbf{u}, \widetilde{\boldsymbol{\rho}}) \in \mathbb{R}^{n\times n}$ is the nonlinear system matrix. We apply a nested approach, where the outer optimization is solved within steepest-descent iterations and the nested magnetostatic problem is eliminated by the Newton method, as described in Algorithm 1. We denote by $I : \mathbb{R}^n \to \mathbb{R}$ the discretized cost functional and by the matrix $\mathbf{A}'_{\mathbf{u}}(\mathbf{u}, \widetilde{\boldsymbol{\rho}})$ we denote the linearization of the mapping $\mathbf{u} \mapsto \mathbf{A}(\mathbf{u}, \widetilde{\boldsymbol{\rho}}) \cdot \mathbf{u}$. In the optimization we choose the initial value of $\boldsymbol{\rho}$ to be 0.5 uniformly in Ω_{d}.

Concerning some numerical results in 2d, for simplicity we consider only two coils to be active and take, due to the symmetry, a quarter of the domain, see Fig. 3. In Fig. 4 there are 2d (a quarter of the geometry) and 3d (an eigth of the geometry) optimal designs depicted for the electromagnet benchmark problem. The 2d problem was solved for 55104 design and 66877 state variables using the multilevel method described below. The 3d problem was solved for 14000 design variables and 33323 state ones. Let us note that we have not employed any regularization technique yet, however, referring to Fig. 4 (left) it seems to be useful.

2.2 Sensitivity analysis

For the outer steepest-descent iterations we have to provide the derivative of the cost functional I subject to the elementwise constant design material function $\boldsymbol{\rho}$.

Algorithm 1 Solving the nonlinear state problem

Given $\boldsymbol{\rho}$, $\widetilde{\boldsymbol{\rho}} := \widetilde{\rho}(\boldsymbol{\rho})$
$i := 0$
Solve $\mathbf{A}(\mathbf{0}, \widetilde{\boldsymbol{\rho}}) \cdot \mathbf{u}^0 = \mathbf{f}$
Assemble $\mathbf{f}^0 := \mathbf{f} - \mathbf{A}(\mathbf{u}^0, \widetilde{\boldsymbol{\rho}})$
while $\|\mathbf{f}^i\|/\|\mathbf{f}\| >$ precision **do**
  $i := i + 1$
  Solve $\mathbf{A}'_{\mathbf{u}}(\mathbf{u}^{i-1}, \widetilde{\boldsymbol{\rho}}) \cdot \mathbf{w}^i = \mathbf{f}^{i-1}$
  Line search $\tau^i := \operatorname{argmin}_\tau \left\|\mathbf{f} - \mathbf{A}(\mathbf{u}^{i-1} + \tau \mathbf{w}^i, \widetilde{\boldsymbol{\rho}})\right\|$
  $\mathbf{u}^i := \mathbf{u}^{i-1} + \tau^i \mathbf{w}^i$
  $\mathbf{f}^i := \mathbf{f} - \mathbf{A}(\mathbf{u}^i, \widetilde{\boldsymbol{\rho}})$
  Store $\mathbf{w}^i$ and τ^i
end while
Store $\mathbf{u}^i$
Store $k := i$
Calculate objective $I(\mathbf{u}^k)$

To this end we differentiate (by hand) Algorithm 1, which results in Algorithm 2. There we additionaly introduce the following matrices:

$$\begin{aligned}
\mathbf{G}_{\widetilde{\boldsymbol{\rho}}}(\mathbf{u}, \mathbf{w}, \widetilde{\boldsymbol{\rho}}) := &- \left(\frac{\partial \mathbf{A}'_{\mathbf{u}}(\mathbf{u}, \widetilde{\boldsymbol{\rho}})}{\partial \rho_1} \cdot \mathbf{w}, \dots, \frac{\partial \mathbf{A}'_{\mathbf{u}}(\mathbf{u}, \widetilde{\boldsymbol{\rho}})}{\partial \rho_m} \cdot \mathbf{w} \right) \\
&- \left(\frac{\partial \mathbf{A}(\mathbf{u}, \widetilde{\boldsymbol{\rho}})}{\partial \rho_1} \cdot \mathbf{u}, \dots, \frac{\partial \mathbf{A}(\mathbf{u}, \widetilde{\boldsymbol{\rho}})}{\partial \rho_m} \cdot \mathbf{u} \right),
\end{aligned}$$

$$\begin{aligned}
\mathbf{G}_{\mathbf{u}}(\mathbf{u}, \mathbf{w}, \widetilde{\boldsymbol{\rho}}) := &- \left(\frac{\partial \mathbf{A}'_{\mathbf{u}}(\mathbf{u}, \widetilde{\boldsymbol{\rho}})}{\partial u_1} \cdot \mathbf{w}, \dots, \frac{\partial \mathbf{A}'_{\mathbf{u}}(\mathbf{u}, \widetilde{\boldsymbol{\rho}})}{\partial u_n} \cdot \mathbf{w} \right) \\
&- \left(\frac{\partial \mathbf{A}(\mathbf{u}, \widetilde{\boldsymbol{\rho}})}{\partial u_1} \cdot \mathbf{u}, \dots, \frac{\partial \mathbf{A}(\mathbf{u}, \widetilde{\boldsymbol{\rho}})}{\partial u_n} \cdot \mathbf{u} \right) - \mathbf{A}(\mathbf{u}, \widetilde{\boldsymbol{\rho}}),
\end{aligned}$$

$$\mathbf{H}_{\widetilde{\boldsymbol{\rho}}}(\mathbf{u}, \widetilde{\boldsymbol{\rho}}) := - \left(\frac{\partial \mathbf{A}(\mathbf{0}, \widetilde{\boldsymbol{\rho}})}{\partial \rho_1} \cdot \mathbf{u}, \dots, \frac{\partial \mathbf{A}(\mathbf{0}, \widetilde{\boldsymbol{\rho}})}{\partial \rho_m} \cdot \mathbf{u} \right).$$

In Fig. 5 there is the nonlinear reluctivity for an optimized design depicted. We can see that only the pole heads, as being close to the coils, behave nonlinearly. There is no difference between the optimal topologies when considering linear and nonlinear state problems. This is probably due to the fact that the cost functional is evaluated outside the ferromagnetic domain.

2.3 Multilevel issues

Let us now consider the linear magnetostatic state problem. We use a coupling of the outer steepest-descent (SD) optimization iterations with the nested Newton

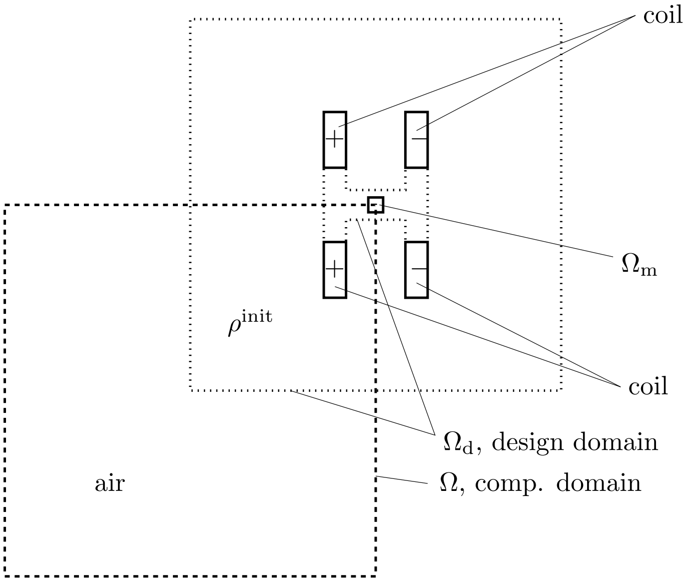

Figure 3: Topology optimization: initial design

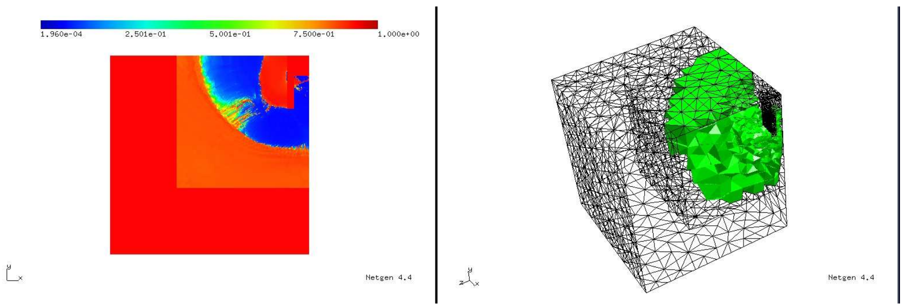

Figure 4: Optimal 2d and 3d shapes

method for the nonlinear state problem. The idea is to use the information about the coarsely optimized design as well as to use the coarse grid preconditioner for all the arising linear systems, see Algorithm 3. At each level the coarse grid preconditioner for the linear system $\mathbf{A}^l(\mathbf{0}, \widetilde{\boldsymbol{\rho}}^l_{\mathrm{opt}})$ at the optimized design is frozen.

From some numerical simulations we observed that the design had hardly changed when starting too far from the intermediate value 0.5, see the locking effect in Fig. 6. Therefore, we had to shrink the optimal coarse design to a small interval close to 0.5 and use this as the initial guess at the next level. Unfortunately, it makes the coarse preconditioner useless in some first iterations of the steepest descent at this actual level. The algorithm is then still quite

Algorithm 2 Adjoint Newton method for the nonlinear state problem

Given $\boldsymbol{\rho}$, $\widetilde{\boldsymbol{\rho}} := \widetilde{\rho}(\boldsymbol{\rho})$, k, $\mathbf{u}^k$, $\{\mathbf{w}^i\}_{i=1}^k$ and $\{\tau^i\}_{i=1}^k$ stored by Algorithm 1
$\boldsymbol{\lambda} := I'_{\mathbf{u}}(\mathbf{u}^k)$
$\boldsymbol{\omega} := \mathbf{0}$
for $i = k, \ldots, 1$ **do**
  $\mathbf{u}^{i-1} := \mathbf{u}^i - \tau^i \mathbf{w}^i$
  Solve $\mathbf{A}'_{\mathbf{u}}(\mathbf{u}^{i-1}, \widetilde{\boldsymbol{\rho}})^T \cdot \boldsymbol{\eta} = \boldsymbol{\lambda}$
  Assemble $\boldsymbol{\omega} := \boldsymbol{\omega} + \tau^i \mathbf{G}_{\widetilde{\boldsymbol{\rho}}}(\mathbf{u}^{i-1}, \mathbf{w}^i, \widetilde{\boldsymbol{\rho}})^T \cdot \boldsymbol{\eta}$
  Assemble $\boldsymbol{\lambda} := \boldsymbol{\lambda} + \tau^i \mathbf{G}_{\mathbf{u}}(\mathbf{u}^{i-1}, \mathbf{w}^i, \widetilde{\boldsymbol{\rho}})^T \cdot \boldsymbol{\eta}$
end for
Solve $\mathbf{A}(\mathbf{0}, \widetilde{\boldsymbol{\rho}})^T \cdot \boldsymbol{\eta} = \boldsymbol{\lambda}$
Assemble $\boldsymbol{\omega} := \boldsymbol{\omega} + \mathbf{H}_{\widetilde{\boldsymbol{\rho}}}(\mathbf{u}^0, \widetilde{\boldsymbol{\rho}})^T \cdot \boldsymbol{\eta}$
Calculate the gradient of the objective $I'_{\boldsymbol{\rho}}(\mathbf{u}^k(\widetilde{\rho}(\boldsymbol{\rho}))) := \widetilde{\rho}'_{\boldsymbol{\rho}}(\boldsymbol{\rho}) \cdot \boldsymbol{\omega}$

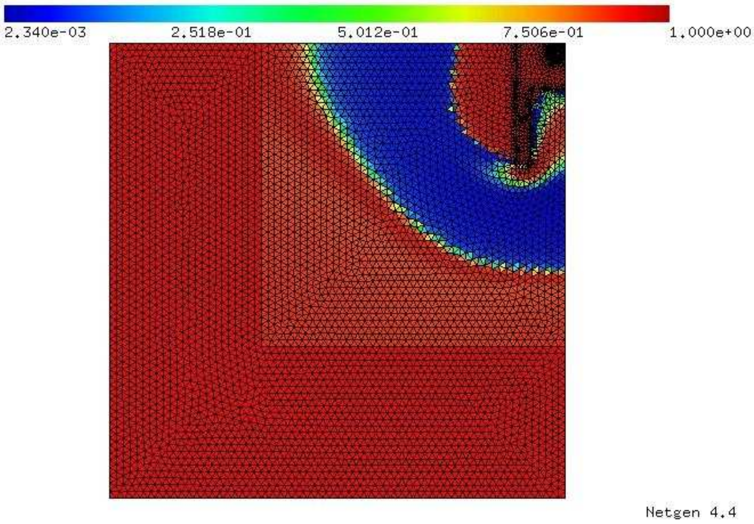

Figure 5: Nonlinear magnetic reluctivity

effective in 2d, see Tables 1, 2, however, yet we have not managed to do so in 3d. This motivates us to focus our effort on applying shape optimization after a coarsely optimized topology design is available.

3 Geometry Handling

The main issue of this topic is to find a proper hirarchical geometric representation and related numerical techniques for dealing with shapes of the structures which arise from topology optimization. Here we mainly cooperate with the

Algorithm 3 Steepest descent iterations coupled with nested Newton-multigrid

Discretize at the first level $\rightsquigarrow h^1, \boldsymbol{\rho}^1_{\text{init}}, \widetilde{\boldsymbol{\rho}}^1_{\text{init}} := \widetilde{\rho}(\boldsymbol{\rho}^1_{\text{init}})$
Solve by (SD) and the nested Newton method-direct solver $\rightsquigarrow \widetilde{\boldsymbol{\rho}}^1_{\text{opt}}$
Store the first level preconditioner $\mathbf{C}^1_{\text{opt}} := \mathbf{A}^1(\mathbf{0}, \widetilde{\boldsymbol{\rho}}^1_{\text{opt}})^{-1}$
for $l = 2, 3, \ldots$ **do**
  Refine $h^{l-1} \rightsquigarrow h^l$
  Increase the penalty p
  Prolong $\boldsymbol{\rho}^{l-1}_{\text{opt}} \rightsquigarrow \boldsymbol{\rho}^l_{\text{init}}, \widetilde{\boldsymbol{\rho}}^l_{\text{init}} := \widetilde{\rho}(\boldsymbol{\rho}^l_{\text{init}})$
  Solve by (SD) and the nested Newton-multigrid solver, using $\mathbf{C}^{l-1}_{\text{opt}} \rightsquigarrow \widetilde{\boldsymbol{\rho}}^l_{\text{opt}}$
  Store the l-th level preconditioner $\mathbf{C}^l_{\text{opt}} \approx \mathbf{A}^l(\mathbf{0}, \widetilde{\boldsymbol{\rho}}^l_{\text{opt}})^{-1}$
end for

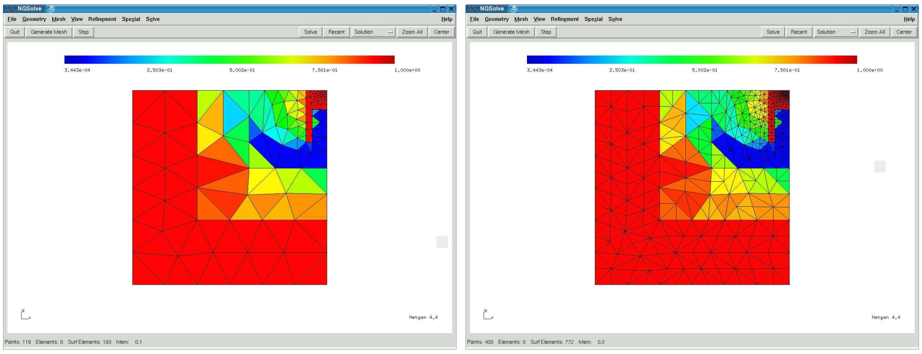

Figure 6: Locking in the coarsely optimized design

subproject F1315. So far we had several meetings with Bert Jüttler, Mohamed Shalaby, and Pavel Chalmovianský and discussed preliminary results. A joint paper with Pavel Chalmovianský is in preparation, see Lukáš and Chalmovianský [11]

3.1 Implicit shape representation using B-spline wavelets

First, we attempted to use implicit representation of the shapes which gives us a strong connection between topology and shape optimization as well as to the level-set methods. The research was initiated by Ph.D. thesis Shalaby [14]. He provides techniques for implicitization of shapes using tensor-product B-splines. Moreover, a hierarchical representation of complex 2d geometries is supported by means of wavelet techniques. In Shalaby [14] he also presents a hierarchical construction which starts from the finest geometry and the details (wavelet coefficients) are neglected at coarser levels. Still, since within our multilevel framework we proceed from the coarse to finest geometry, one has to develop a method the other way round. One can use a p-refinement of the

level	design vars.	state vars.	SD iters.	PCG iters. (rel. prec. 10^{-2})	total time
1	3920	4832	9		12s
2	15680	19021	9	4–7	31s
3	62720	75473	9	4–7	3min 57s
4	250880	300673	11	12–19	14min 10s

Table 1: Multilevel 2d topology optimization governed with linear magnetostatics

level	design vars.	state vars.	SD iters.	PCG iters. linear/linearized	total time
1	3920	4832	9		1min 6s
2	15680	19021	9	5–7/17–32	3min 21s
3	62720	75473	9	4–7/19–49	19min 45s
4	250880	300673	23	11–18/25–64	4h 17min 8s

Table 2: Multilevel 2d topology optimization governed with nonlinear magnetostatics

B-splines, see Fig. 7, however, the hierarchy then is not nested. Therefore, we prefer an h-refinement when using a low order, e.g. bilinear B-splines.

It is natural to use this representation with a level-set-type method. After several meetings with Martin Burger, we started to work on using the phase field method. In particular, we only added the following phase field penalization term to the objective:

$$\mathcal{P}_p(\rho) := p \int_{\Omega_\mathrm{d}} \rho^2(1-\rho^2)\, d\mathbf{x} + \frac{1}{p}\int |\mathbf{grad}(\rho)|^2\, d\mathbf{x}.$$

The first term penalizes the intermediate values instead of the arctan-like penalization $\widetilde{\rho}_p(\rho)$, the second one is a perimeter penalty. However, this method had taken too long before the convergence was achieved. Typically, after 800 iterations the method was still in progress with the intermediate results depicted in Fig. 8. Moreover, one has to tune sensitively the value of the phase field penalty p with respect to the penalty of the inequality constraints in (1) and (2) or (3), respectively. A similar numerical evidence was also observed by Martin Burger. Due to that our work concerning the phase field method as well as implicit shape representations has stalled.

3.2 Parameteric shape representation using Bézier curves

Next, we discussed the geometric issues with Pavel Chalmovianský and we realized that Bézier curves or surfaces have two nice properties that make them

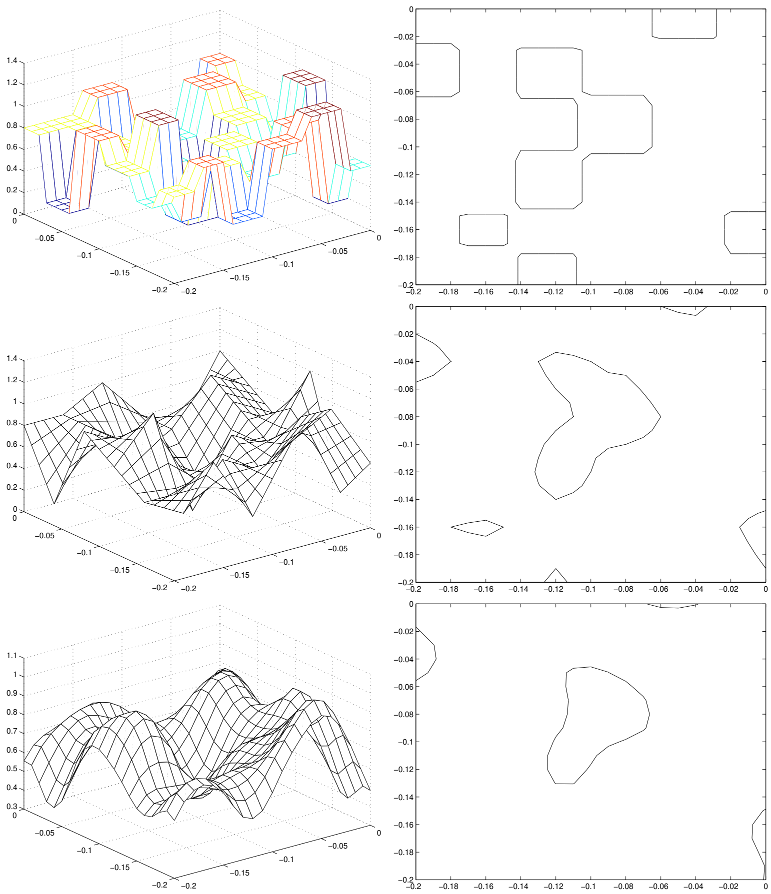

Figure 7: B-spline implicit shape representation of the order 0, 1, 2 and their 0-level sets

superior to be used. First, one can introduce new control nodes so that the Bézier curve or surface is the same, thus, we have a nested hierarchy of them. Second, just a few such refinements makes the control polygon close enough to the Bézier shape. Therefore, it is sufficient to work with the polygons. In Fig. 9 there are 3d pole heads of the electromagnet modelled by the Bézier surfaces.

3.3 Approximation of shapes arising from 2d topology optimization

Another issue that has been tackled is an integration of topology and shape optimization. First we want to solve a rather coarsely discretized topology optimization problem, then, we identify the boundary and/or interfaces of the

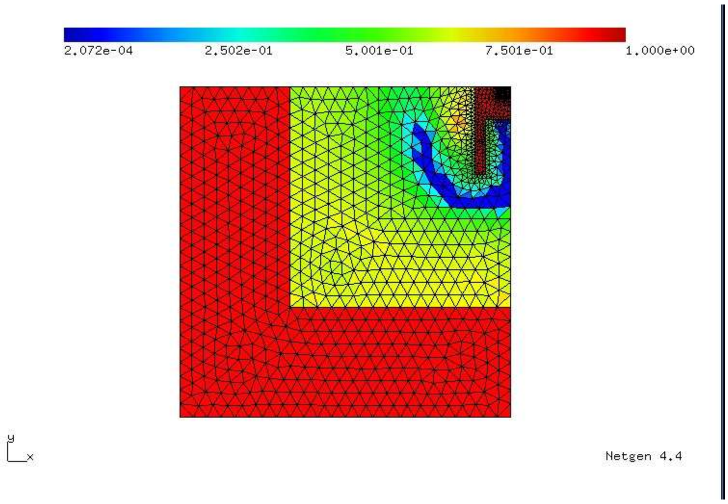

Figure 8: Design development after 800 iterations of the phase field method

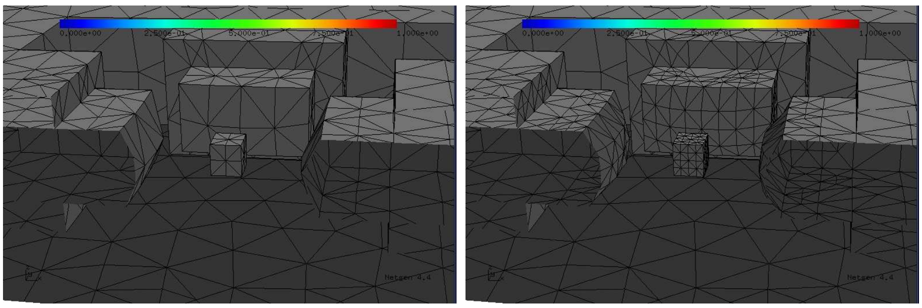

Figure 9: Pole heads modelled by Bézier surfaces in a nested hierarchy

resulting structure, approximate the shapes using the Bézier parameterization, and finally, proceed on with the multilevel shape optimization.

The first step towards a fully automatic procedure is a shape identification, which we are doing by hand for the moment. The second step we are treating now is a piecewise smooth approximation of the shapes by Bézier curves. Let $\rho^{\mathrm{opt}} \in \mathcal{Q}$ be an optimized discretized material distribution. Recall that it is not a strictly 0-1 function. Let $\mathbf{p}_1 \in \mathbb{R}^{n_1}, \ldots, \mathbf{p}_s \in \mathbb{R}^{n_s}$ denote vectors of Bézier parameters of the shapes $\alpha_1(\mathbf{p}_1), \ldots, \alpha_s(\mathbf{p}_s)$ which form the air and ferromagnetic subdomains $\Omega_0(\alpha_1, \ldots, \alpha_s)$, $\Omega_1(\alpha_1, \ldots, \alpha_s)$, respectively, where $\Omega_1 \subset \Omega_{\mathrm{d}}$, $\overline{\Omega} = \overline{\Omega_0} \cup \overline{\Omega_1}$ and $\Omega_0 \cap \Omega_1 = \emptyset$. Let further $\underline{\mathbf{p}_i}$ and $\overline{\mathbf{p}_i}$ denote the lower and upper bounds, respectively, and let

$$\mathcal{P} := \big\{ (\mathbf{p}_1, \ldots, \mathbf{p}_s) \mid \underline{\mathbf{p}_i} \leq \mathbf{p}_i \leq \overline{\mathbf{p}_i} \text{ for } i = 1, \ldots, s \big\} \tag{4}$$

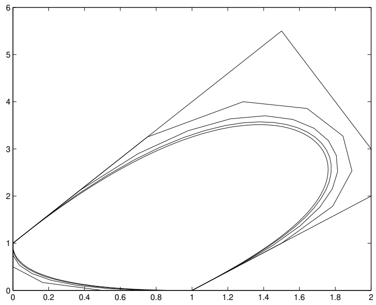

Figure 10: Approximation of Bézier shapes by the refined control polygon

be the set of admissible Bézier parameters. We solve the following least square fitting problem:

$$\min_{(\mathbf{p}_1,\dots,\mathbf{p}_s)\in\mathcal{P}} \int_{\Omega_\mathrm{d}} \left(\rho^{\mathrm{opt}} - \chi(\Omega_1\left(\alpha_1(\mathbf{p}_1),\dots,\alpha_s(\mathbf{p}_s)\right))\right)^2 \, d\mathbf{x}, \tag{5}$$

where $\chi(\Omega_1)$ is the characteristic function of Ω_1.

When solving (5) numerically, one encounters a problem of intersection of the Bézier shapes with the mesh on which ρ^{opt} is elementwise constant. In order to avoid it we use the property that the Bézier control polygon converges quite fast to the curve under the following refinement procedure:

$$\begin{aligned} [\mathbf{p}_i^{\mathrm{new}}]_1 &:= [\mathbf{p}_i]_1 \,, \\ [\mathbf{p}_i^{\mathrm{new}}]_j &:= \tfrac{j-1}{n_i+1}\,[\mathbf{p}_i]_{j-1} + \tfrac{n_i-j}{n_i+1}\,[\mathbf{p}_i]_j \,,\ j=2,\dots,n_i, \\ [\mathbf{p}_i^{\mathrm{new}}]_{n_i+1} &:= [\mathbf{p}_i]_{n_i} \,, \end{aligned} \tag{6}$$

where $i = 1,\dots,s$. This procedure adds one control node so that the resulting Bézier shape remains unchanged. In Fig. 10 a convergence of control polygons of 6, 11, 21, 41 and 81 nodes to the Bézier shape is depicted. Note that in 3d one uses a similar procedure provided a tensor-product grid of Bézier control nodes. Then the integration in (5) is replaced by a sum over the elements and we deal with intersecting of the mesh and a polygon.

Note that the least square functional in (5) is not differentiable whenever a shape touches the grid. However, we compute forward finite differences, which is still acceptable for the steepest-descent optimization method that we apply. The smoothness can be achieved by smoothing the characteristic function $\chi(\Omega_1)$.

Numerical experiments are depicted in Fig. 11. Here we have 19 design parameters in total and solving the least square problem (5) was finished in 8 steepest-descent iterations, which took 26 seconds when using the numerical differentiation.

Note also that a similar topic has recently appeared in the F1306 project, see Nübel, Düster, and Rank [12].

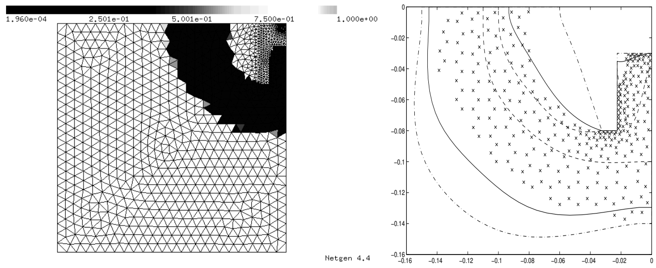

Figure 11: Smooth shapes fitting: **(a)** coarsely optimized design ρ^{opt}; **(b)** dashed line – lower bound; dash-and-dot line – upper bound; solid line – smooth shape approximation; crosses – mid-points of the elements with $\rho^{\text{opt}} \geq 0.5$

4 Shape Optimization

Considering the notation in (2) and (4), we have the following shape optimization problem governed now with the 3d linear magnetostatics:

$$\left\{\begin{array}{lr} \displaystyle\min_{(\mathbf{p}_1,\dots,\mathbf{p}_s)\in\mathcal{P}} \mathcal{I}\left(\mathbf{curl}(\mathbf{u}), \alpha_1(\mathbf{p}_1), \dots, \alpha_s(\mathbf{p}_s)\right) & \\ \text{w.r.t.} & \\ \displaystyle\int_{\Omega_0(\alpha_1(\mathbf{p}_1),\dots,\alpha_s(\mathbf{p}_s))} \nu_0 \mathbf{curl}(\mathbf{u})\cdot\mathbf{curl}(\mathbf{v})\,d\mathbf{x} & \\ \displaystyle\quad + \int_{\Omega_1(\alpha_1(\mathbf{p}_1),\dots,\alpha_s(\mathbf{p}_s))} \nu_1 \mathbf{curl}(\mathbf{u})\cdot\mathbf{curl}(\mathbf{v})\,d\mathbf{x} & \\ \displaystyle\quad = \int_\Omega \mathbf{J}\cdot\mathbf{v}\,d\mathbf{x} \text{ in } \mathbf{H}_{0,\perp}(\mathbf{curl};\Omega). & \end{array}\right. \tag{7}$$

Similarly to the problem (3), we can introduce a 2d reduced shape optimization problem. The problems are discretized by means of the finite element method using the proper lowest order finite elements. The mesh is deformed in accordance to the shape changes by means of solution to an artificial discretized linear elasticity problem. In Fig. 12 you can see the 2d and 3d optimized shapes of the pole heads of the electromanget.

4.1 SQP method coupled with geometric multigrid

The multilevel algorithm here is similar to Algorithm 3, while now we use the sequential quadratic programming (SQP) instead of the steepest-descent outer iterations. The numerical performance for the 3d problem is presented in Table 3, the resulting optimized shape of the pole head is depicted in Fig. 12. Note that there was also a 0-th level, where we only assembled the coarsest grid preconditioner for the initial design which is then efficiently used by the multigrid. Note also that the computational time will be much improved after we implement the adjoint method of the shape sensitivity analysis instead of the numerical differentiation.

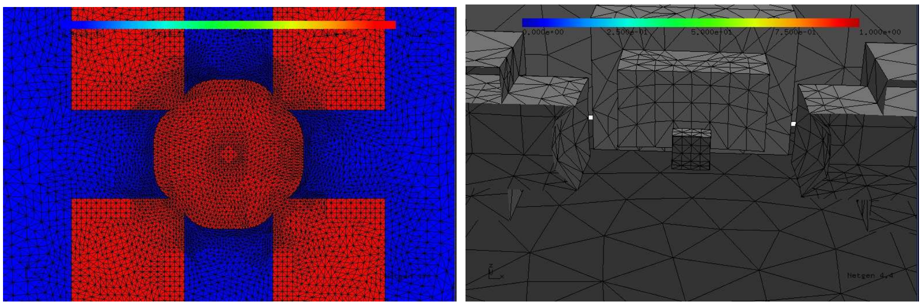

Figure 12: Optimal 2d and 3d shapes of the pole heads of the electromagnet

level	design vars.	state vars.	SQP iters.	PCG iters. (rel. prec. 10^{-2})	total time
1	4	17653	2	3	4min
2	16	34750	2	3	8min
3	64	93265	2	3	1h 7min

Table 3: SQP method coupled with multigrid for 3d shape optimization

4.2 A sequential coupling of coarse topology and multilevel shape optimization

Here we are motivated by Chang and Tang [16], where they apply a similar algorithm as we do to structural mechanics, however, using re-meshing in a CAD software environment, which was computationally expensive. Our aim here is to make the algorithm fast. Therefore, we additionally employ a multilevel method.

We take the smooth shape from Fig. 11 and proceed further with shape optimization in a multilevel way. In Fig. 13 there is the resulting geometry as well as a picture of the so-called O-ring electromagnet, which was manufactured at the Institute of Physics, TU Ostrava, some years ago. Without any a priori information about the shape, we approved the fact, well-known in the engineering community, that round geometries of electromagnets are superior. Numerical performance of the multilevel shape optimization algorithm is drawn in Table 4.

The method will be further applied to develop electromagnets for 3d spatial controlled homogeneous magnetic field, where there is a lack of knowledge on the construction, and for optimal shield design of a transformer in order to minimize the eddy current losses, which has arisen in a project of Joachim Schöberl.

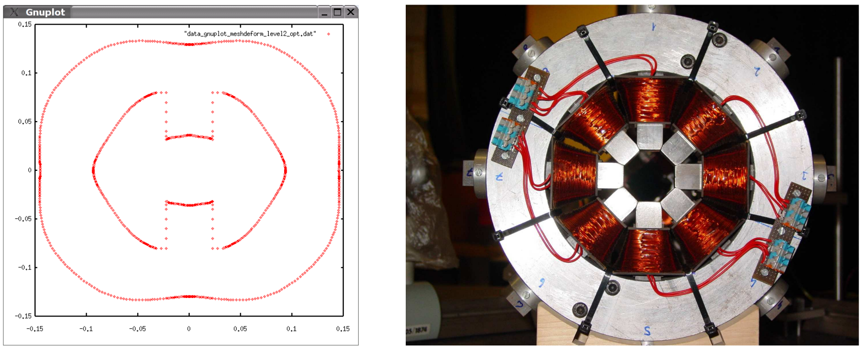

Figure 13: Sequential topology-shape optimization: **(a)** 2d optimized geometry; **(b)** O-ring electromagnet

level	design vars.	state vars.	SQP iters.	PCG iters. (rel. prec. 10^{-2})	total time
1	19	1098	9		28s
2	40	4240	10	3–4	3min 30s
3	82	16659	12	4–5	34min 28s

Table 4: Multilevel 2d topology-shape optimization using mesh deformation

4.3 A composite finite-element approach

We are motivated by Sauter and Hackbusch [5, 4], where they introduce finite elements that resolve fine details in the geometry. Our aim here is to generalize this approach for optimal design. We already implemented a kind of 2d finite elements for shape optimization so that the polygonal shape is allowed to cross the elements, thus, there are jumps in the material function within some elements. Then the computational grid is fixed and we do not need to deal with the shape-to-mesh mapping and consequently with the degenerated or even flipped elements. Unfortunately, this approach causes bad convergence properties of the geometric multigrid we use, see Table 5. Another drawback is that the assembling of the system matrix takes long due to the resolving the intersection of elements with a design polygon.

4.4 Newton method coupled with algebraic multigrid

This is a cooperation in a very progess with Johannes Kraus, RICAM. The goal here is to replace the geometric multigrid by an algebraic (AMG) one and use it together with the kind of composite finite-element approach described above. We started with the 2d Poisson system and generated three typical matrices at a given discretization, but with different shapes, and we are constructing one

level	design vars.	state vars.	SD iters.	PCG iters. (rel. prec. 10^{-2})	total time
1	19	1098	14		4min 32s
2	40	4240	6	11–14	26min 37s
3	82	16659	3	21–25	3h 20min 15s

Table 5: Multilevel 2d topology-shape optimization with shapes across elements

common AMG preconditioner for them. A similar test will be done for 3d curl-curl system matrices. The cooperation will run further. We believe that AMG is better suited for the shape optimization problems.

4.5 A symbolical approach to sensitivity analysis

Here we are motivated by Hazra and Schulz [6], where they perform Fourier analysis of the symbol of a reduced Hessian and they constructed a preconditioner based on an approximation of the inverse operator to the reduced Hessian. They consider the all-at-once optimization. This symbolical approach is equivalent to the classical shape sensitivity analysis, see Sokolowski and Zolesio [15]. It works unless the state equation is nonlinear. One can apply the technique to optimal boundary control or optimal shape design, unfortunately, not to topology optimization.

We describe briefly the analysis technique, as it is presented in Hazra and Schulz [6] or Arian and Ta'asan [1], and apply it to our 2d shape optimization problem governed with the linear Poisson equation. Let (u^*, Γ^*) denote a couple of the state solution and optimal shape design interface. We choose a point $\mathbf{x}_0 \in \Gamma^*$ and we localize and linearize the optimization problem in a vicinity of $\mathbf{x}_0$, which leads to a problem defined in $\mathbb{R}^2$, where Γ^* is replaced by the axis $\mathbb{R} \times \{0\}$. The domain above $\mathbb{R}^2_+ := \mathbb{R} \times \{y > 0\}$ is occupied by the ferromagnetics and the domain below $\mathbb{R}^2_- := \mathbb{R} \times \{y < 0\}$ is the air subdomain. We further introduce a perturbation $\widetilde{\alpha}$ of the shape and the related state perturbations $\widetilde{u}$ as follows:

$$\Gamma = \Gamma^* + \varepsilon\widetilde{\alpha}\mathbf{n}, \quad u_0 = u_0^* + \varepsilon\widetilde{u_0} + O(\varepsilon^2), \quad u_1 = u_1^* + \varepsilon\widetilde{u_1} + O(\varepsilon^2),$$

where $\mathbf{n} := (0, 1)$ is the normal vector to the linearized Γ^* and where u_0 and u_1 are the solutions to the following strongly formulated 2d linear magnetostatic system:

$$\begin{aligned}
-\mathrm{div}(\nu_0 \nabla u_0) &= J \text{ in } \Omega_0(\Gamma^*),\\
-\mathrm{div}(\nu_1 \nabla u_1) &= 0 \text{ in } \Omega_1(\Gamma^*),\\
((u_0)'_y, -(u_0)'_x) \cdot \mathbf{n} &= ((u_1)'_y, -(u_1)'_x) \cdot \mathbf{n} \text{ on } \Gamma^*,\\
\nu_0 \nabla u_0 \cdot \mathbf{n} &= \nu_1 \nabla u_1 \cdot \mathbf{n} \text{ on } \Gamma^*\\
u &\to 0 \text{ as } \|(x, y)\| \to \infty.
\end{aligned}$$

Then we are to solve the following small state perturbance problem:

$$
\begin{aligned}
-\triangle\widetilde{u_0} &= 0 \text{ in } \mathbb{R}^2_-, \\
-\triangle\widetilde{u_1} &= 0 \text{ in } \mathbb{R}^2_+, \\
(\widetilde{u_0})'_x - (\widetilde{u_1})'_x &= \widetilde{\alpha}'_x[(u_1)'_y - (u_0)'_y] + \widetilde{\alpha}[(u_1)''_{yx} - (u_0)''_{yx}] \text{ on } \mathbb{R}^2_0, \\
\nu_0(\widetilde{u_0})'_y - \nu_1(\widetilde{u_1})'_y &= \widetilde{\alpha}[\nu_1(u_1)''_{yy} - \nu_0(u_0)''_{yy}] \text{ on } \mathbb{R}^2_0, \\
\widetilde{u_0}, \widetilde{u_1} &\rightarrow 0 \text{ as } y \rightarrow \infty.
\end{aligned}
$$

Next, we apply the local mode analysis. We assume one mode of the shape perturbation given as follows:

$$\widetilde{\alpha}(x) := \widehat{\widetilde{\alpha}}(\omega_x)\mathrm{e}^{\mathrm{i}\omega_x x}$$

and we are looking for the related state perturbations in the form

$$\widetilde{u_{0(1)}}(x,y) := \widehat{\widetilde{u_{0(1)}}}(\omega_x, \omega_{0(1)y})\widehat{\widetilde{\alpha}}(\omega_x)\mathrm{e}^{\mathrm{i}\omega_x x}\mathrm{e}^{\mathrm{i}\omega_{0(1)y} y}.$$

Substituting this ansatz to the above small perturbance shape problem, we get the following two quadratic equations to be solved symbolically for ω_{0y} and ω_{1y}, respectively:

$$(\omega_x)^2 + (\omega_{0(1)y})^2 = 0$$

and we get the following system of two linear equations:

$$\begin{pmatrix} \mathrm{i}\omega_x & -\mathrm{i}\omega_x \\ \nu_0\mathrm{i}\omega_{0y} & -\nu_1\mathrm{i}\omega_{1y} \end{pmatrix} \begin{pmatrix} \widehat{\widetilde{u_0}} \\ \widehat{\widetilde{u_1}} \end{pmatrix} = \begin{pmatrix} \mathrm{i}\omega_x[(u_1)'_y - (u_0)'_y] + [(u_1)''_{yx} - (u_1)''_{yx}] \\ \nu_1(u_1)''_{yy} - \nu_0(u_0)''_{yy} \end{pmatrix}.$$

The far field condition together with the ansatz imply that the solutions ω_{0y} and ω_{1y} are imaginary and positive, therefore, unique.

Finally, the symbol of the reduced Hessian arises after the derivative of the perturbed solutions $\widetilde{u_{0(1)}}$ with respect to the shape perturbation $\widetilde{\alpha}$. Then, the backward Fourier transformation leads to a second order elliptic PDE operator.

Our goal was to establish a cooperation with a symbolical SFB subproject and apply a symbolical solver to the system of polynomials. However, when considering the 2nd order PDE operators the presented Fourier analysis leads to simple quadratic equations.

4.6 Symmetries

We were looking with Nicoletta Bila for a use of symmetries for a dimensional reduction of the strong formulation of the magnetostatic state problem. The reduction is based on Fourier analysis, so we cannot consider a nonconstant material coefficient function. Dr. Bila can deal with geometrical symmetries, e.g. cylindrical, for which, however, the analytical solution is well-known from physics. Finally, we found useful to compare analytical solutions of the curl-curl Maxwell system and the regularized (perturbed) system curl-curl + ε, which is often used for numerical calculation instead of the original curl-curl system. From the analysis it might be useful to have some a priori information on choosing the regularization parameter ε. Dr. Bila presents more details in an SFB report.

5 Software

We have provided the following new functionality to Netgen/NgSolve: extension of Netgen by Bézier curves; extension of NgSolve with sensitivity analysis for nonlinear state problems, BDB integrators for topology optimization governed with nonlinear state problems, computational geometry tools (2d Bézier polygons, refinement, intersection with the grid), refinement of marked subdomains and surfaces. It remains to incorporate all the tools from the author's version of the Netgen/NgSolve to the public one. We are, together with Joachim Schöberl, still be looking for a way of the incorporation so that the current code will remain unchanged.

Soon, we will add to Netgen/NgSolve Bézier patches defined on a triangle and rectangle, computational geometry tools for them and BDB integrators for shape optimization governed with nonlinear state problems.

References

[1] E. Arian and S. Ta'asan. Analysis of the Hessian for aerodynamic optimization: Inviscid flow. Technical report, NASA.

[2] M. P. Bendsøe. *Optimization of Structural Topology, Shape and Material*. Springer, Berlin, Heidelberg, 1995.

[3] T. Borrvall. *Computational Topology Optimization of Elastic Continua by Design Restrictions*. PhD thesis, Linköping University, Sweden, 2000.

[4] W. Hackbusch and S. A. Sauter. Composite finite elements for problems containing small geometric details - part II: Implementation and numerical results. *Comput. Vis. Sci.*, 1:15–25, 1997.

[5] W. Hackbusch and S. A. Sauter. Composite finite elements for the approximation of PDEs on domains with complicated micro–structures. *Numer. Math.*, 75:447–472, 1997.

[6] S.B. Hazra and V. Schulz. Simultaneous pseudo-timestepping for pde-model based optimization problems. *BIT*, 2004. In print.

[7] M. Křížek and P. Neittaanmäki. *Mathematical and Numerical Modelling in Electrical Engineering*. Kluwer Academic Publishers, Dordrecht, 1996.

[8] D. Lukáš. Shape optimization of homogeneous electromagnets. In Ursula van Rienen, Michael Günther, and Dirk Hecht, editors, *Scientific Computing in Electrical Engineering*, volume 18 of *Lect. Notes Comp. Sci. Eng.*, pages 145–152. Springer, 2001.

[9] D. Lukáš. On solution to an optimal shape design problem in 3-dimensional magnetostatics. *Appl. Math.*, 49(5):441–464, 2004.

[10] D. Lukáš. An integration of optimal topology and shape design for magnetostatics. In *Proceedings of "Scientific Computing in Electrical Engineering 2004"*. Submitted.

[11] D. Lukáš and P. Chalmovianský. A sequential coupling of optimal topology and shape design applied to 2-dimensional nonlinear magnetostatics. To be submitted to Comp.Vis.Sci.

[12] V. Nübel, A. Düster, and E. Rank. An *rp*–adaptive finite element method for elastoplasic problems. In *ECCOMAS 2004*.

[13] K. Postava, D. Hrabovský, J. Pištora, A. R. Fert, Š Višňovský, and T. Yamaguchi. Anisotropy of quadratic magneto–optic effects in reflection. *J. Appl. Phys.*, 91:7293–7295, 2002.

[14] M. Shalaby. *Spline Implicitization of Planar Shapes and Applications.* PhD thesis, RISC, University Linz, July 2003.

[15] J. Sokolowski and J.-P. Zolesio. *Introduction to Shape Optimization.* Number 16 in Springer Series in Computational Mathematics. Springer, Berlin, 1992.

[16] P.-S. Tang and K.-H. Chang. Integration of topology and shape optimization for design of structural components. *Struct. Multidisc. Optim.*, 22:65–82, 2001.

[17] A. K. Zvedin and V. A. Kotov. *Modern Magnetooptics and Magnetooptical Materials.* Institute of Physics Publishing Bristol and Philadelphia, 1997.